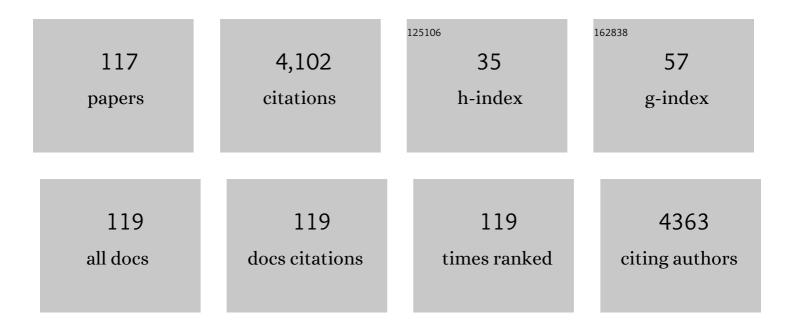
Xionghan Feng

List of Publications by Year in descending order

Source: https://exaly.com/author-pdf/238893/publications.pdf Version: 2024-02-01



#	Article	IF	CITATIONS
1	Co-sorption of metal ions and inorganic anions/organic ligands on environmental minerals: A review. Science of the Total Environment, 2022, 803, 149918.	3.9	44
2	Role of clay minerals in controlling phosphorus availability in a subtropical Alfisol. Geoderma, 2022, 409, 115592.	2.3	17
3	The effect of citric acid on the catalytic oxidation of Mn(II) on ferrihydrite surface. Applied Geochemistry, 2022, 139, 105262.	1.4	4
4	Mechanisms of efficient As(III) and As(V) removal by Ni-coprecipitated hausmannite nanocomposites. Journal of Environmental Chemical Engineering, 2022, 10, 107684.	3.3	0
5	The impacts of aging pH and time of acid mine drainage solutions on Fe mineralogy and chemical fractions of heavy metals in the sediments. Chemosphere, 2022, 303, 135077.	4.2	12
6	Effect and fate of Ni during aging and thermal-induced phyllomanganate-to-tectomanganate transformation. Geochimica Et Cosmochimica Acta, 2022, 333, 200-215.	1.6	2
7	Effects of particle size and mineral crystallinity on formation of Zn Al layered double hydroxides (LDH) on aluminum (oxyhydr)oxides. Applied Clay Science, 2021, 201, 105933.	2.6	3
8	As(<scp>iii</scp>) adsorption–oxidation behavior and mechanisms on Cr(<scp>vi</scp>)-incorporated schwertmannite. Environmental Science: Nano, 2021, 8, 1593-1602.	2.2	7
9	Transformation of the phyllomanganate vernadite to tectomanganates with small tunnel sizes: Favorable geochemical conditions and fate of associated Co. Geochimica Et Cosmochimica Acta, 2021, 295, 224-236.	1.6	12
10	Molecular-Scale Understanding of Sulfate Exchange from Schwertmannite by Chromate Versus Arsenate. Environmental Science & Technology, 2021, 55, 5857-5867.	4.6	35
11	Facet-Dependent Photoinduced Transformation of Cadmium Sulfide (CdS) Nanoparticles. Environmental Science & Technology, 2021, 55, 13132-13141.	4.6	5
12	Kinetics of Mn(II) adsorption and catalytic oxidation on the surface of ferrihydrite. Science of the Total Environment, 2021, 791, 148225.	3.9	18
13	Adsorption and precipitation of <i>myo</i> â€inositol hexakisphosphate onto kaolinite. European Journal of Soil Science, 2020, 71, 226-235.	1.8	16
14	Preference of Co over Al for substitution of Fe in goethite (α-FeOOH) structure: Mechanism revealed from EXAFS, XPS, DFT and linear free energy correlation model. Chemical Geology, 2020, 532, 119378.	1.4	14
15	Effects of Co(II) ion exchange, Ni(II)- and V(V)-doping on the transformation behaviors of Cr(III) on hexagonal turbostratic birnessite-water interfaces. Environmental Pollution, 2020, 256, 113462.	3.7	17
16	Transformation of Ni-containing birnessite to tectomanganate: Influence and fate of weakly bound Ni(II) species. Geochimica Et Cosmochimica Acta, 2020, 271, 96-115.	1.6	11
17	Coupled morphological and structural evolution of δ-MnO ₂ to α-MnO ₂ through multistage oriented assembly processes: the role of Mn(<scp>iii</scp>). Environmental Science: Nano, 2020, 7, 238-249.	2.2	10
18	Modeling coupled kinetics of arsenic adsorption/desorption and oxidation in ferrihydrite-Mn(II)/manganese (oxyhydr)oxides systems. Chemosphere, 2020, 244, 125517.	4.2	9

#	Article	IF	CITATIONS
19	Oxidation of Mn(III) Species by Pb(IV) Oxide as a Surrogate Oxidant in Aquatic Systems. Environmental Science & Technology, 2020, 54, 14124-14133.	4.6	17
20	Highly enhanced oxidation of arsenite at the surface of birnessite in the presence of pyrophosphate and the underlying reaction mechanisms. Water Research, 2020, 187, 116420.	5.3	17
21	Synergistic effect of Co(II) doping on FeS activating heterogeneous Fenton processes toward degradation of Rhodamine B. Chemical Engineering Journal Advances, 2020, 4, 100044.	2.4	8
22	Effects of Al substitution on local structure and morphology of lepidocrocite and its phosphate adsorption kinetics. Geochimica Et Cosmochimica Acta, 2020, 276, 109-121.	1.6	27
23	Formation and transformation of schwertmannite through direct Fe ³⁺ hydrolysis under various geochemical conditions. Environmental Science: Nano, 2020, 7, 2385-2398.	2.2	14
24	The alkaline photo-sulfite system triggers Fe(IV/V) generation at hematite surfaces. Chemical Engineering Journal, 2020, 401, 126124.	6.6	20
25	Quantitative investigation of ZnO nanoparticle dissolution in the presence of δ-MnO2. Environmental Science and Pollution Research, 2020, 27, 14751-14762.	2.7	3
26	Adsorption of Cr(VI) on Al-substituted hematites and its reduction and retention in the presence of Fe2+ under conditions similar to subsurface soil environments. Journal of Hazardous Materials, 2020, 390, 122014.	6.5	43
27	The Speciation of Cd in Cd–Fe Coprecipitates: Does Cd Substitute for Fe in Goethite Structure?. ACS Earth and Space Chemistry, 2019, 3, 2225-2236.	1.2	20
28	Effects of myo-inositol hexakisphosphate, ferrihydrite coating, ionic strength and pH on the transport of TiO2 nanoparticles in quartz sand. Environmental Pollution, 2019, 252, 1193-1201.	3.7	11
29	Phosphate Sorption Speciation and Precipitation Mechanisms on Amorphous Aluminum Hydroxide. Soil Systems, 2019, 3, 20.	1.0	36
30	Truncated octahedral bipyramidal TiO ₂ /MXene Ti ₃ C ₂ hybrids with enhanced photocatalytic H ₂ production activity. Nanoscale Advances, 2019, 1, 1812-1818.	2.2	63
31	Effects of Mn ²⁺ , Ni ²⁺ , and Cu ²⁺ on the Formation and Transformation of Hydrosulfate Green Rust: Reaction Processes and Underlying Mechanisms. ACS Earth and Space Chemistry, 2019, 3, 519-530.	1.2	14
32	The catalytic effect of AQDS as an electron shuttle on Mn(II) oxidation to birnessite on ferrihydrite at circumneutral pH. Geochimica Et Cosmochimica Acta, 2019, 247, 175-190.	1.6	19
33	Transformation of Co-containing birnessite to todorokite: Effect of Co on the transformation and implications for Co mobility. Geochimica Et Cosmochimica Acta, 2019, 246, 21-40.	1.6	38
34	Formation of Zn-Al layered double hydroxides (LDH) during the interaction of ZnO nanoparticles (NPs) with γ-Al2O3. Science of the Total Environment, 2019, 650, 1980-1987.	3.9	28
35	A Quantitative Model for the Coupled Kinetics of Arsenic Adsorption/Desorption and Oxidation on Manganese Oxides. Environmental Science and Technology Letters, 2018, 5, 175-180.	3.9	44
36	Quantification of Coexisting Inner- and Outer-Sphere Complexation of Sulfate on Hematite Surfaces. ACS Earth and Space Chemistry, 2018, 2, 387-398.	1.2	43

#	Article	IF	CITATIONS
37	Kinetics of heavy metal adsorption and desorption in soil: Developing a unified model based on chemical speciation. Geochimica Et Cosmochimica Acta, 2018, 224, 282-300.	1.6	93
38	Binding Geometries of Silicate Species on Ferrihydrite Surfaces. ACS Earth and Space Chemistry, 2018, 2, 125-134.	1.2	27
39	Efficient catalytic As(III) oxidation on the surface of ferrihydrite in the presence of aqueous Mn(II). Water Research, 2018, 128, 92-101.	5.3	66
40	Modeling of Cd adsorption to goethite-bacteria composites. Chemosphere, 2018, 193, 943-950.	4.2	31
41	Enhanced photocatalytic H2-production activity of C-dots modified g-C3N4/TiO2 nanosheets composites. Journal of Colloid and Interface Science, 2018, 513, 866-876.	5.0	178
42	Aging shapes the distribution of copper in soil aggregate size fractions. Environmental Pollution, 2018, 233, 569-576.	3.7	38
43	Effect of Cd and Al Coincorporation on the Structures and Properties of Goethite. ACS Earth and Space Chemistry, 2018, 2, 1283-1293.	1.2	8
44	Effects of <i>Myo</i> -inositol Hexakisphosphate on Zn(II) Sorption on γ-Alumina: A Mechanistic Study. ACS Earth and Space Chemistry, 2018, 2, 787-796.	1.2	15
45	The preferential retention of VIZn over IVZn on birnessite during dissolution/desorption. Applied Clay Science, 2018, 161, 169-175.	2.6	8
46	In situ ATR-FTIR spectroscopic study of the co-adsorption of myo-inositol hexakisphosphate and Zn(II) on goethite. Soil Research, 2018, 56, 526.	0.6	7
47	Adsorption of glycerophosphate on goethite (αâ€FeOOH): A macroscopic and infrared spectroscopic study. Journal of Plant Nutrition and Soil Science, 2018, 181, 557-565.	1.1	15
48	Catalytic oxidation of arsenite and reaction pathways on the surface of CuO nanoparticles at a wide range of pHs. Geochemical Transactions, 2018, 19, 12.	1.8	14
49	Mechanisms of Mn(II) catalytic oxidation on ferrihydrite surfaces and the formation of manganese (oxyhydr)oxides. Geochimica Et Cosmochimica Acta, 2017, 211, 79-96.	1.6	100
50	Distinct effects of Al3+ doping on the structure and properties of hexagonal turbostratic birnessite: A comparison with Fe3+ doping. Geochimica Et Cosmochimica Acta, 2017, 208, 268-284.	1.6	26
51	Self-assembly of birnessite nanoflowers by staged three-dimensional oriented attachment. Environmental Science: Nano, 2017, 4, 1656-1669.	2.2	24
52	Effects of polyphosphates and orthophosphate on the dissolution and transformation of ZnO nanoparticles. Chemosphere, 2017, 176, 255-265.	4.2	28
53	Phosphate and phytate adsorption and precipitation on ferrihydrite surfaces. Environmental Science: Nano, 2017, 4, 2193-2204.	2.2	81
54	Local structure of Cu2+ in Cu-doped hexagonal turbostratic birnessite and Cu2+ stability under acid treatment. Chemical Geology, 2017, 466, 512-523.	1.4	31

#	Article	IF	CITATIONS
55	Rapid determination of the Mn average oxidation state of Mn oxides with a novel two-step colorimetric method. Analytical Methods, 2017, 9, 103-109.	1.3	40
56	Influences and Mechanisms of As(V) Concentration and Environmental Factors on Hydrosulfate Green Rust Transformation. Acta Chimica Sinica, 2017, 75, 608.	0.5	4
57	Effects of myo-inositol hexakisphosphate and orthophosphate adsorption on aggregation of CeO2 nanoparticles: roles of pH and surface coverage. Environmental Chemistry, 2016, 13, 34.	0.7	8
58	Preparation and characterization of biocompatible molecularly imprinted poly(ionic liquid) films on the surface of multi-walled carbon nanotubes. RSC Advances, 2016, 6, 43526-43538.	1.7	21
59	Enhanced Dissolution and Transformation of ZnO Nanoparticles: The Role of Inositol Hexakisphosphate. Environmental Science & Technology, 2016, 50, 5651-5660.	4.6	60
60	The associations of heavy metals with crystalline iron oxides in the polluted soils around the mining areas in Guangdong Province, China. Chemosphere, 2016, 161, 181-189.	4.2	82
61	Competitive adsorption of Pb and Cd on bacteria–montmorillonite composite. Environmental Pollution, 2016, 218, 168-175.	3.7	71
62	Mechanisms on the morphology variation of hematite crystals by Al substitution: The modification of Fe and O reticular densities. Scientific Reports, 2016, 6, 35960.	1.6	43
63	Size-controlled synthesis and formation mechanism of manganese oxide OMS-2 nanowires under reflux conditions with KMnO 4 and inorganic acids. Solid State Sciences, 2016, 55, 152-158.	1.5	13
64	Surface speciation of myo-inositol hexakisphosphate adsorbed on TiO2 nanoparticles and its impact on their colloidal stability in aqueous suspension: A comparative study with orthophosphate. Science of the Total Environment, 2016, 544, 134-142.	3.9	24
65	Surface adsorption and precipitation of inositol hexakisphosphate on calcite: A comparison with orthophosphate. Chemical Geology, 2016, 421, 103-111.	1.4	34
66	Effects of Al3+ doping on the structure and properties of goethite and its adsorption behavior towards phosphate. Journal of Environmental Sciences, 2016, 45, 18-27.	3.2	31
67	Redox Reactions between Mn(II) and Hexagonal Birnessite Change Its Layer Symmetry. Environmental Science & Technology, 2016, 50, 1750-1758.	4.6	102
68	Effects of crystallite size on the structure and magnetism of ferrihydrite. Environmental Science: Nano, 2016, 3, 190-202.	2.2	77
69	The Presence of Ferrihydrite Promotes Abiotic Formation of Manganese (Oxyhydr)oxides. Soil Science Society of America Journal, 2015, 79, 1297-1305.	1.2	35
70	Formation of todorokite from "c-disordered―H+-birnessites: the roles of average manganese oxidation state and interlayer cations. Geochemical Transactions, 2015, 16, 8.	1.8	25
71	Desorption ofmyo-inositol hexakisphosphate and phosphate from goethite by different reagents. Journal of Plant Nutrition and Soil Science, 2015, 178, 878-887.	1.1	20
72	Interaction mechanisms and kinetics of ferrous ion and hexagonal birnessite in aqueous systems. Geochemical Transactions, 2015, 16, 16.	1.8	22

#	Article	IF	CITATIONS
73	Absorption mechanisms of Cu2+ on a biogenic bixbyite-like Mn2O3 produced by Bacillus CUA isolated from soil. Geochemical Transactions, 2015, 16, 5.	1.8	6
74	Structure and properties of Co-doped cryptomelane and its enhanced removal of Pb 2+ and Cr 3+ from wastewater. Journal of Environmental Sciences, 2015, 34, 77-85.	3.2	30
75	Structure and properties of vanadium(V)-doped hexagonal turbostratic birnessite and its enhanced scavenging of Pb2+ from solutions. Journal of Hazardous Materials, 2015, 288, 80-88.	6.5	30
76	Sulfate Local Coordination Environment in Schwertmannite. Environmental Science & Technology, 2015, 49, 10440-10448.	4.6	77
77	High Co-doping promotes the transition of birnessite layer symmetry from orthogonal to hexagonal. Chemical Geology, 2015, 410, 12-20.	1.4	27
78	Oxidation process of dissolvable sulfide by synthesized todorokite in aqueous systems. Journal of Hazardous Materials, 2015, 290, 106-116.	6.5	24
79	Fe-doped cryptomelane synthesized by refluxing at atmosphere: Structure, properties and photocatalytic degradation of phenol. Journal of Hazardous Materials, 2015, 296, 221-229.	6.5	46
80	Size-dependent sorption of myo-inositol hexakisphosphate and orthophosphate on nano-γ-Al2O3. Journal of Colloid and Interface Science, 2015, 451, 85-92.	5.0	33
81	Formation and secondary mineralization of ferrihydrite in the presence of silicate and Mn(II). Chemical Geology, 2015, 415, 37-46.	1.4	52
82	Effects of phosphate and silicate on the transformation of hydroxycarbonate green rust to ferric oxyhydroxides. Geochimica Et Cosmochimica Acta, 2015, 171, 1-14.	1.6	27
83	Microcalorimetric Study on the Growth and Metabolism of a Manganese-Oxidizing Bacterium and its Mutant Strain. Geomicrobiology Journal, 2015, 32, 585-593.	1.0	1
84	Transformation from Phyllomanganates to Todorokite under Various Conditions: A Review of Implication for Formation Pathway of Natural Todorokite. ACS Symposium Series, 2015, , 107-134.	0.5	4
85	Adsorption-Desorption of Myo-Inositol Hexakisphosphate on Hematite. Soil Science, 2014, 179, 476-485.	0.9	28
86	Zn sorption to biogenic bixbyite-like Mn 2 O 3 produced by Bacillus CUA isolated from soil: XAFS study with constraints on sorption mechanism. Chemical Geology, 2014, 389, 82-90.	1.4	18
87	Mechanism of Myo-inositol Hexakisphosphate Sorption on Amorphous Aluminum Hydroxide: Spectroscopic Evidence for Rapid Surface Precipitation. Environmental Science & Technology, 2014, 48, 6735-6742.	4.6	103
88	Effects of Co and Ni co-doping on the structure and reactivity of hexagonal birnessite. Chemical Geology, 2014, 381, 10-20.	1.4	66
89	Solid-State NMR Spectroscopic Study of Phosphate Sorption Mechanisms on Aluminum (Hydr)oxides. Environmental Science & Technology, 2013, 47, 130725144353009.	4.6	30
90	Transformation of hydroxycarbonate green rust into crystalline iron (hydr)oxides: Influences of reaction conditions and underlying mechanisms. Chemical Geology, 2013, 351, 57-65.	1.4	36

#	Article	IF	CITATIONS
91	Effect of Ferrihydrite Crystallite Size on Phosphate Adsorption Reactivity. Environmental Science & Technology, 2013, 47, 10322-10331.	4.6	191
92	Effects of Fe doping on the structures and properties of hexagonal birnessites – Comparison with Co and Ni doping. Geochimica Et Cosmochimica Acta, 2013, 117, 1-15.	1.6	71
93	Characteristics of Phosphate Adsorption-Desorption Onto Ferrihydrite. Soil Science, 2013, 178, 1-11.	0.9	155
94	Fourier transform infrared spectroscopy study of acid birnessites before and after Pb ²⁺ adsorption. Clay Minerals, 2012, 47, 191-204.	0.2	44
95	Role of Counteranions in Sol–Gel-Derived Alkoxyl-Functionalized Ionic-Liquid-Based Organic–Inorganic Hybrid Coatings for SPME. Chromatographia, 2012, 75, 1421-1433.	0.7	20
96	Sorption behavior of heavy metals on birnessite: Relationship with its Mn average oxidation state and implications for types of sorption sites. Chemical Geology, 2012, 292-293, 25-34.	1.4	157
97	Characterization of Ni-rich hexagonal birnessite and its geochemical effects on aqueous Pb2+/Zn2+ and As(III). Geochimica Et Cosmochimica Acta, 2012, 93, 47-62.	1.6	83
98	Synthesis of hureaulite by a reflux process at ambient temperature and pressure. Microporous and Mesoporous Materials, 2012, 153, 115-123.	2.2	17
99	Large-scale size-controlled synthesis of cryptomelane-type manganese oxide OMS-2 in lateral and longitudinal directions. Journal of Materials Chemistry, 2011, 21, 5223.	6.7	23
100	Co2+-exchange mechanism of birnessite and its application for the removal of Pb2+ and As(III). Journal of Hazardous Materials, 2011, 196, 318-326.	6.5	48
101	α-MnO2 nanowires transformed from precursor δ-MnO2 by refluxing under ambient pressure: The key role of pH and growth mechanism. Materials Chemistry and Physics, 2011, 125, 678-685.	2.0	32
102	Oxidation behavior and kinetics of sulfide by synthesized manganese oxide minerals. Journal of Soils and Sediments, 2011, 11, 1323-1333.	1.5	22
103	Characterization of Co-doped birnessites and application for removal of lead and arsenite. Journal of Hazardous Materials, 2011, 188, 341-349.	6.5	70
104	Effect of 1-1 electrolyte concentration on the adsorption/desorption of copper ion on synthetic birnessite. Journal of Soils and Sediments, 2010, 10, 879-885.	1.5	11
105	Aging promotes todorokite formation from layered manganese oxide at near-surface conditions. Journal of Soils and Sediments, 2010, 10, 1540-1547.	1.5	16
106	Shapeâ€controlled Synthesis of Nanostructure Ramsdelliteâ€type Manganese Oxide at Atmospheric Pressure. Chinese Journal of Chemistry, 2010, 28, 2301-2307.	2.6	3
107	Cobalt-doped todorokites prepared by refluxing at atmospheric pressure as cathode materials for Li batteries. Electrochimica Acta, 2010, 55, 9157-9165.	2.6	18
108	Synthesis of a Nanofibrous Manganese Oxide Octahedral Molecular Sieve with Co(NH ₃) ₆ ³⁺ Complex Ions as a Template via a Reflux Method. Crystal Growth and Design, 2010, 10, 3355-3362.	1.4	11

#	Article	IF	CITATIONS
109	Factors Governing the Formation of Lithiophorite at Atmospheric Pressure. Clays and Clay Minerals, 2009, 57, 353-360.	0.6	10
110	Relationship Between Pb ²⁺ Adsorption and Average Mn Oxidation State in Synthetic Birnessites. Clays and Clay Minerals, 2009, 57, 513-520.	0.6	71
111	Relation of lead adsorption on birnessites with different average oxidation states of manganese and release of Mn2+/H+/K+. Journal of Environmental Sciences, 2009, 21, 520-526.	3.2	26
112	Synthesis of todorokite-type manganese oxide from Cu-buserite by controlling the pH at atmospheric pressure. Microporous and Mesoporous Materials, 2009, 117, 41-47.	2.2	23
113	Birnessites with Different Average Manganese Oxidation States Synthesized, Characterized, and Transformed to Todorokite at Atmospheric Pressure. Clays and Clay Minerals, 2009, 57, 715-724.	0.6	41
114	Influence of Mn(III) availability on the phase transformation from layered buserite to tunnel-structured todorokite. Clays and Clay Minerals, 2008, 56, 397-403.	0.6	45
115	Pathways of birnessite formation in alkali medium. Science in China Series D: Earth Sciences, 2005, 48, 1438-1451.	0.9	34
116	Factors governing formation of todorokite at atmospheric pressure. Science in China Series D: Earth Sciences, 2005, 48, 1678-1689.	0.9	10
117	Synthesis of todorokite by refluxing process and its primary characteristics. Science in China Series D: Earth Sciences, 2004, 47, 760-768.	0.9	9